Electronic Supplementary Material (ESI) for Environmental Science: Nano.

Simultaneous removal of arsenite and cadmium by manganese-crosslinking sodium alginate modified biochar and zerovalent iron composite from aqueous solutions

Wei Mao,[ab] Lixun Zhang,*[abc] Ying Zhang,[ab] and Yuntao Guan*[ab]

[a] Guangdong Provincial Engineering Technology Research Center for Urban Water Cycle and Water Environment Safety, Tsinghua Shenzhen International Graduate School, Tsinghua University, Shenzhen 518055, P.R. China

[b] State Environmental Protection Key Laboratory of Microorganism Application and Risk Control, School of Environment, Tsinghua University, Beijing 100084, P.R. China

[C] Department of Civil and Environmental Engineering, University of California, Irvine, CA, 92612, United States

*Correspondence

Room 1807, Energy and Environment Building, Tsinghua Shenzhen International Graduate School, Tsinghua University, Shenzhen 518055, China; Email: guanyt@tsinghua.edu.cn (Yuntao Guan), lixunz@uci.edu (Lixun Zhang)

Materials

Forestry waste (Fig. S1) was obtained from Xili University Town located in Guangdong Province, China. Before use, it was selected, dried, and ground into powder (<0.15 mm, sieved). All chemicals involved in the present study were of analytical grade or higher. $AlCl_3$, $CaCl_2$, $FeSO_4{\cdot}7H_2O$, HCl, KCl, $MgCl_2$, $MnSO_4$, $NaBH_4$, NaCl, Na_2CO_3, $NaNO_3$, NaOH, $Na_3PO_4{\cdot}12H_2O$, Na_2SO_4, NH_4Cl, and sodium alginate (SA) were purchased from Aladdin Chemicals Co. Ltd (Shanghai, China). $CdCl_2{\cdot}5/2H_2O$ and $NaAsO_2$ were provided by Sigma-Aldrich Co. Ltd (Shanghai, China). In addition, all solutions were prepared with 18.2 MΩ cm deionized (DI) water produced by Milli-Q (Millipore).

Characterization methods

Scanning electron microscopy with energy dispersion spectrometry (SEM-EDS) of Mn/SA-BC, nZVI, and Mn/SA-BC@nZVI were recorded with the application of an SU8010 SEM (Hitachi, Japan). Elemental composition and valence state of Mn/SA-BC, nZVI, and Mn/SA-BC@nZVI were explored using X-ray photoelectron spectroscopy (XPS) performed by a PHI 5000 VersaProbe II spectrometer (ULVAC-PHI, Japan). X-ray diffraction (XRD) patterns of adsorbents were measured on a D/MAX 2500X-ray diffractometer (Rigaku, Japan) with Cu target in the 2θ range from 10° to 90° (40 kV). Fourier transform infrared spectra (FT-IR) of Mn/SA-BC and Mn/SA-BC@nZVI were acquired by a Nicolet iS50 NIR (Thermo Scientific, USA) with the use of KBr pellets. BET specific surface area and pore size distributions of nZVI and Mn/SA-BC@nZVI were determined by N_2 adsorption-desorption experiments (Belsorp Max, MicrotracBEL, Japan). In addition, electron spin resonance (ESR) result was measured by a JEOL JES-FA200 (ESR/EPR) spectrometer based on spin-trap reagent 5,5-dimethyl-l-pyrroline N-oxide (DMPO).

Adsorption experiments

The adsorption kinetics of As(III) and Cd(II) were investigated by batch experiments based on 15 mg of Mn/SA-BC@nZVI with 30 mL of As(III) or Cd(II) solution (10 mg/L) in 50 mL glass bottle, respectively. Each adsorption experiment was shaken in a thermostatic shaker (SHZ-C, Changzhou, China) at 25°C and 220 rpm for the specified time. Subsequently, the suspensions were passed through a disposable Millipore filter (0.45 um pore size) for performing subsequent analysis using inductively coupled plasma-optical emission spectrometer (ICP-OES) (Optima 7300DV, PerkinElmer, USA). The valence state of As was measured by Dionex ICS-3000 ion chromatography-inductively coupled plasma mass spectrometry (IC-ICP-MS) (Thermo Scientific, USA). The Fe(II) concentrations in the solution were analyzed by UV-vis spectrophotometer (Shimadzu, Kyoto, Japan) at 510 nm by employing the 1,10-phenanthroline method. Pseudo-first-order (Eq. (S1)) and pseudo-second-order (Eq. (S2)) models were applied to investigate the experimental data.[1, 2] The adsorption isotherms of As(III) and Cd(II) on Mn/SA-BC@nZVI were measured with varying initial concentrations of As(III) (5, 10, 30, 50, 100, 150, 200, 300, and 400 mg/L) and Cd(II) (5, 10, 30, 50, 100, 150, 200, 300, and 400 mg/L). Freundlich (Eq. (S3)) and Langmuir (Eq. (S4)) models were adopted to simulate the isotherms data.[3]

The simultaneous removal of As(III) and Cd(II) was determined with Mn/SA-BC@nZVI dosage of 0.5 g/L with 30 mL of working solution. The initial concentration ratios of As(III) and Cd(II) contained 1:1 (10, 10 mg/L), 1:2 (10, 20 mg/L), 1:3 (10, 30 mg/L), 2:1 (20, 10 mg/L), 2:2 (20, 20 mg/L), 2:3 (20, 30 mg/L), 3:1 (30, 10 mg/L), 3:2 (30, 20 mg/L), and 3:3 (30, 30 mg/L). The adsorption kinetics of As(III) (20 mg/L) and Cd(II) (20 mg/L) in a mixed solution were investigated with Mn/SA-BC@nZVI dosage of 0.5 g/L for different time intervals (0-3 h).

The effects of pH on the simultaneous removal of As(III) (20 mg/L) and Cd(II) (20 mg/L) were investigated by performing experiments with initial pH values of 2-10. The pH value was adjusted with 0.1 mol/L NaOH or HCl solution. The effects of coexisting ions (Cl^-, SO_4^{2-}, NO_3^-, PO_4^{3-}, CO_3^{2-}, Mg^{2+}, Ca^{2+}, NH_4^+, K^+, and Al^{3+}) and humic acid on the simultaneous removal of As(III) (20 mg/L) and Cd(II) (20 mg/L) were explored by carrying out batch experiments. Besides, the batch experiments were conducted by the same process as the adsorption kinetic experiments.

Adsorption kinetics models

$$q_t = q_e \times (1 - \exp(-K_1 t)) \quad \text{(S1)}$$

$$\frac{t}{q_t} = \frac{1}{K_2 q_e^2} + \frac{t}{q_e} \quad \text{(S2)}$$

where q_e (mg/g) refers to the adsorption capacity of Mn/SA-BC@nZVI, q_t (mg/g) is the adsorption capacity of Mn/SA-BC@nZVI at time t (min), K_1 (min^{-1}) represents the pseudo-first-order rate constant, and K_2 (g/mg/min) indicates the pseudo-second-order rate constant.

Adsorption isotherm models

$$q_e = \frac{q_m \times b \times C_e}{1 + b + C_e} \quad \text{(S3)}$$

$$q_e = K_f \times C_e^{(1/n)} \quad \text{(S4)}$$

where C_e (mg/L) is the equilibrium concentration, b (L/mg) is the Langmuir bonding term, q_e (mg/g) is the adsorption capacity of Mn/SA-BC@nZVI, q_m (mg/g) is the Langmuir maximum capacity, K_f ($L^n \cdot mg^{(1-n)}/g$) stands for the Freundlich affinity coefficient, and *n* denotes the Freundlich linearity constant.

Table S1. Parameters of pseudo-first-order and pseudo-second-order kinetic models for the adsorption of As(III) and Cd(II) by Mn/SA-BC@nZVI.

Kinetic models		Single solution		Mixed solution	
		As(III)	Cd(II)	As(III)	Cd(II)
pseudo-first-order	R^2	0.900	0.966	0.837	0.945
	$K_1(min^{-1})$	0.087	0.122	0.1724	2.694
	$q_e(mg/g)$	17.963	17.963	32.321	29.135
pseudo-second-order	R^2	0.964	0.989	0.958	0.970
	$K_1(min^{-1})$	0.040	0.023	0.036	0.193
	$q_e(mg/g)$	18.033	18.080	32.680	29.165

Table S2. Isotherm parameters of Langmuir and Freundlich for the adsorption of As(III) and Cd(II) by Mn/SA-BC@nZVI.

Isotherm models		As(III)	Cd(III)
Langmuir	R^2	0.991	0.990
	B(L/mg)	0.012	0.020
	$Q_m(mg/g)$	121.283	120.898
Freundlich	R^2	1	0.999
	K_f	113.541	126.971
	n	7.629	5.409

Table S3. Comparation of the Langmuir maximum capacity (q_m) of carbon-based adsorbents for As(III) and Cd(II).

Absorbents	q_m (mg/g)/equilibrium time(min)		Absorbent dose (g/L)	refs
	As(III)	Cd(II)		
Mn/SA-BC@nZVI	121.28	120.90	0.5	this work
FMBC		95.23	1	[4]
RSB-beads		158.77	0.2	[5]
POSB		46.2	0.2	[6]
Fe/Zn-RBC		98.58	1	[7]
Fe/Zn-DBC		161.14	1	[7]
Ce/Mn binary oxide	97.7		0.2	[8]
Fe-modifies biochar	56.06		2	[9]
Fe-NN/BFs	70.22		1	[10]
ZVI-RO	15.58		1	[11]
$FeCl_3$BC900	5		10	[12]
Fe_3O_4/SS-BC	39.47		2	[13]
MBB	25.04	4.58	2.5	[14]
BCTD	72.62	118.06	1	[15]
nZVI-BC	33.81	148.5	0.25	[16]
GMB	169.0	73.7	0.166	[17]
Ca-MBC1	6.34	10.07	2	[18]

Table S4. Radical concentration of •OH at different times.

Time (min)	Free radical content (spins/mm^3)
0	0
5	$1.042*10^{13}$
10	$2.490*10^{13}$

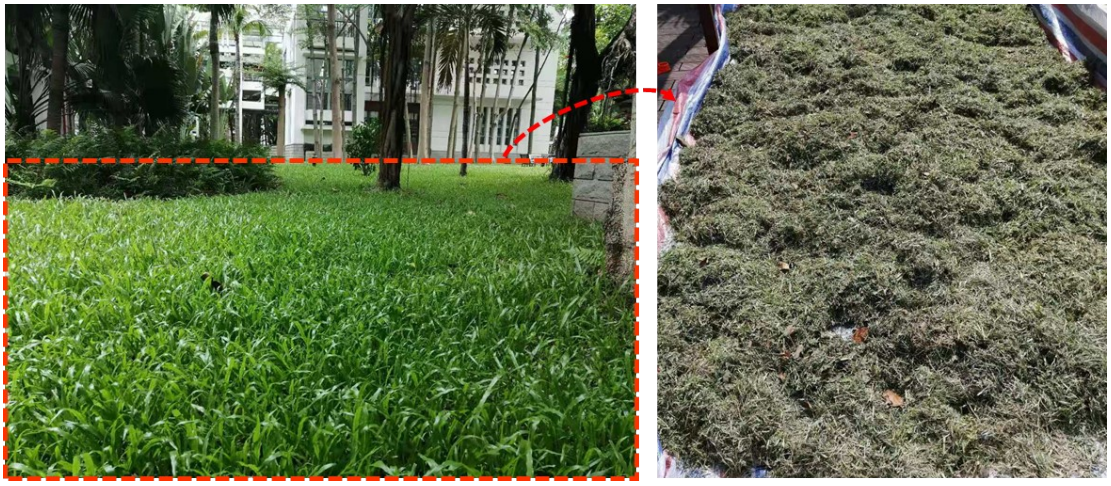

Fig. S1. Schematic diagram of forestry waste.

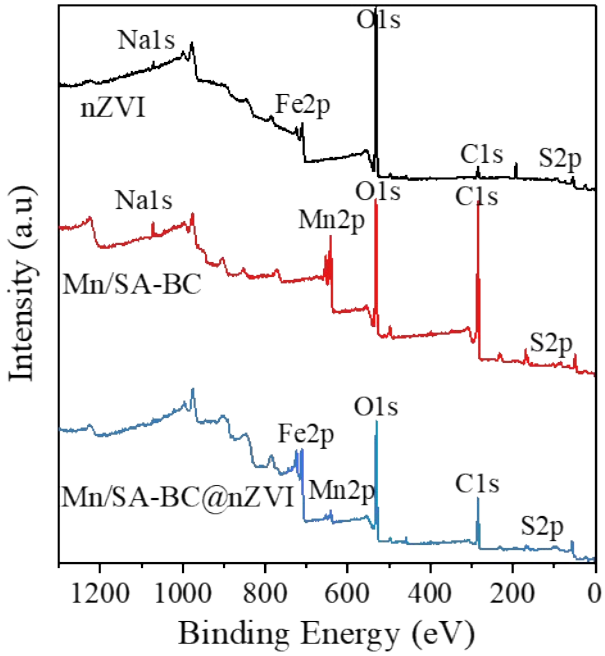

Fig. S2. Wide-scan survey XPS spectra of Mn/SA-BC, nZVI, and Mn/SA-BC@nZVI.

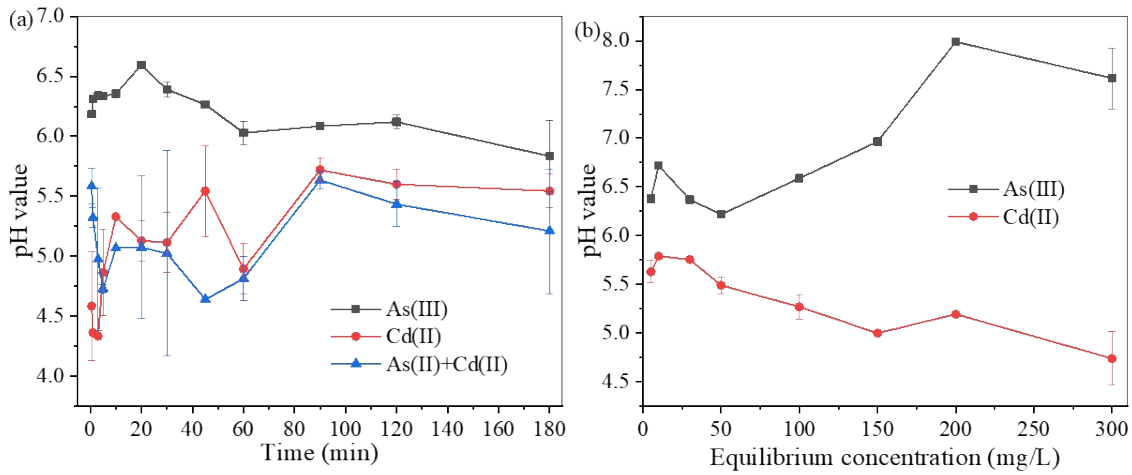

Fig. S3. The pH values of (a) adsorption kinetics and (b) adsorption isotherm solution with Mn/SA-BC@nZVI.

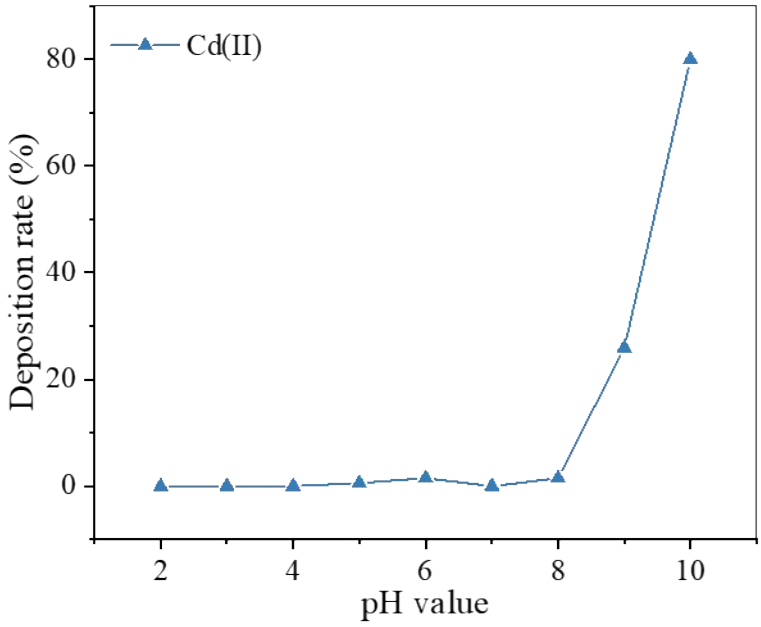

Fig. S4. The deposition rate of Cd(II) with varying pH value.

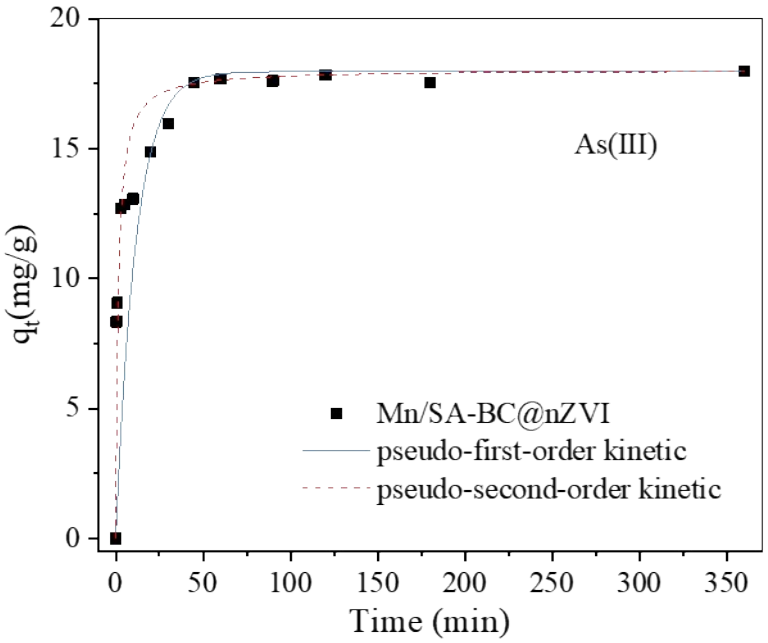

Fig. S5. As(III) adsorption kinetics fitted by pseudo-first-order and pseudo-second-order models.

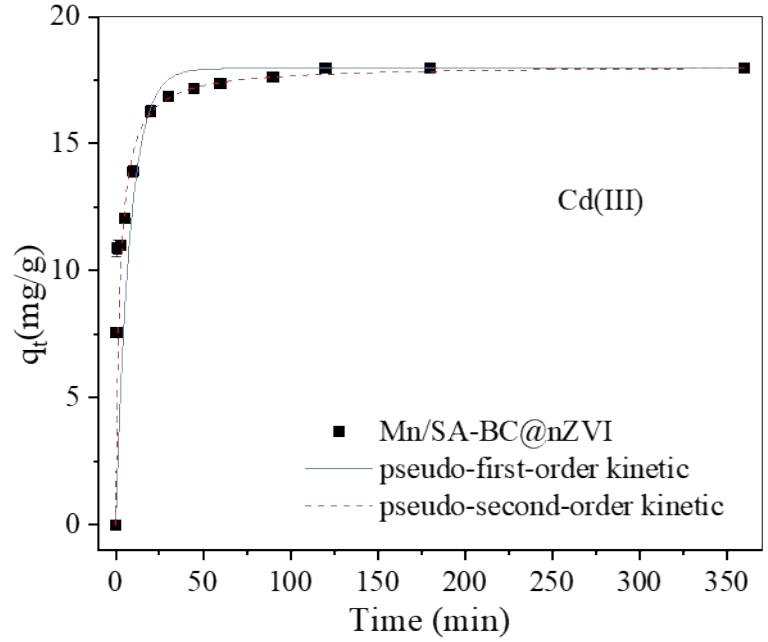

Fig. S6. Cd(II) adsorption kinetics fitted by pseudo-first-order and pseudo-second-order models.

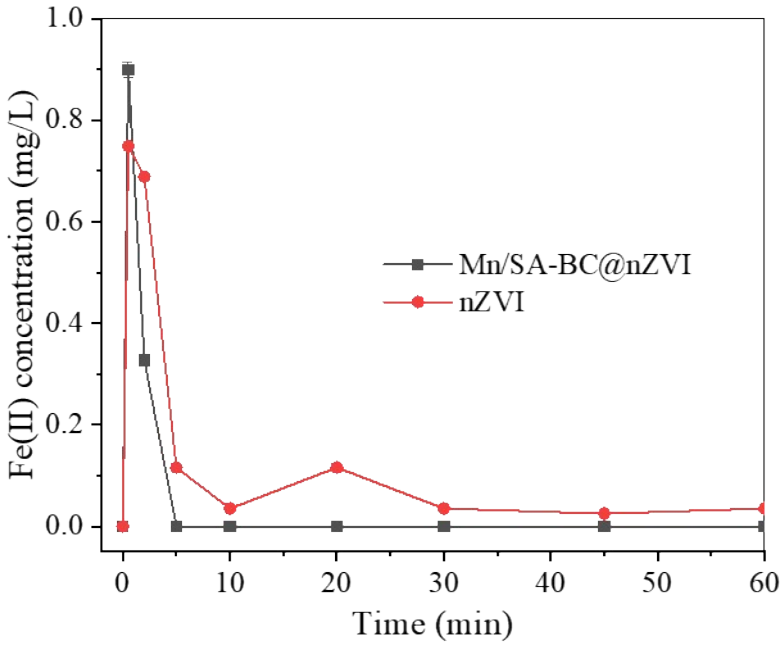

Fig. S7. The release of Fe(II) from nZVI and Mn/SA-BC@nZVI in the reaction system without added As(III) and Cd(II).

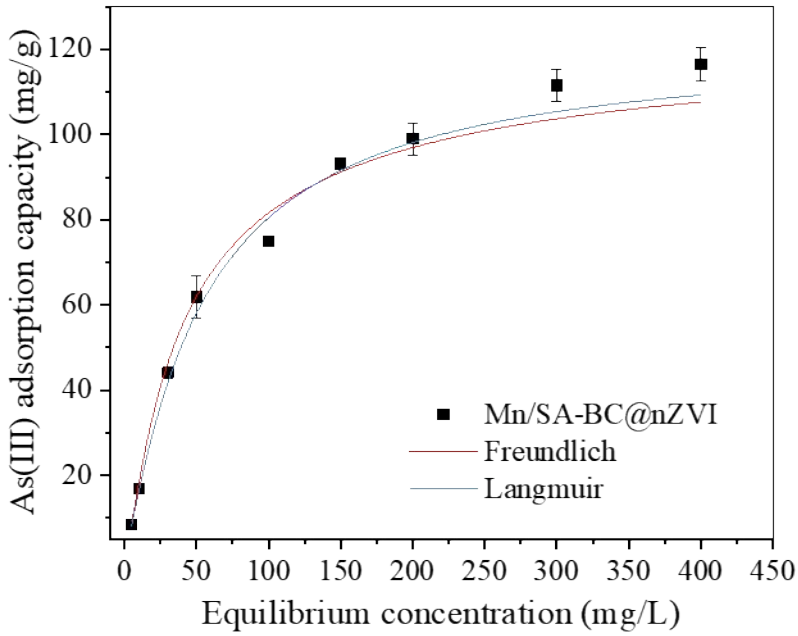

Fig. S8. Adsorption isotherm of As(III) onto the Mn/SA-BC@nZVI with Langmuir and Freundlich equations.

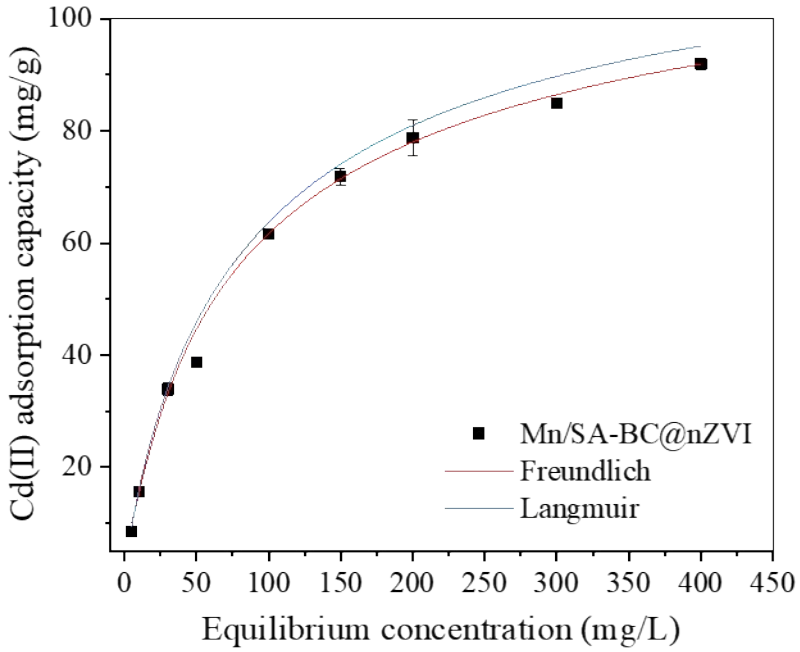

Fig. S9. Adsorption isotherm of Cd(II) onto the Mn/SA-BC@nZVI with Langmuir and Freundlich equations.

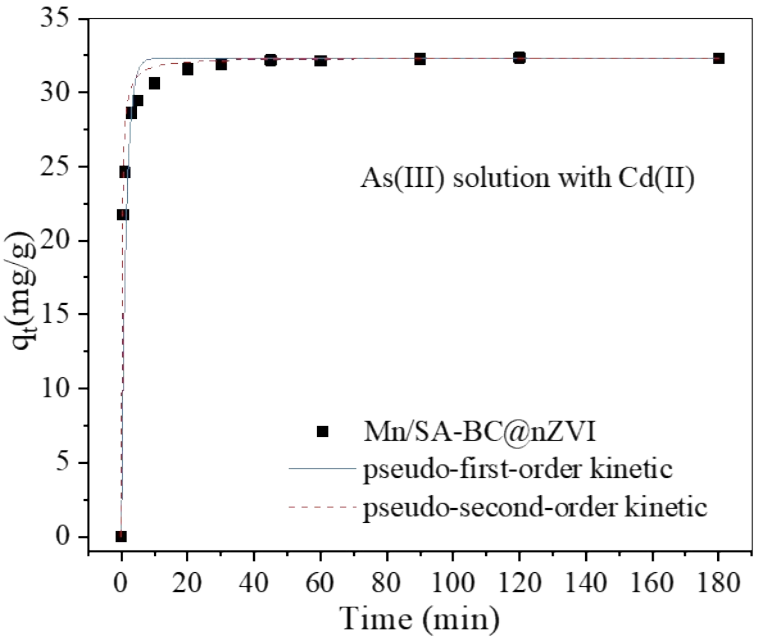

Fig. S10. As(III) adsorption kinetics fitted of mixed solution system by pseudo-first-order and pseudo-second-order models.

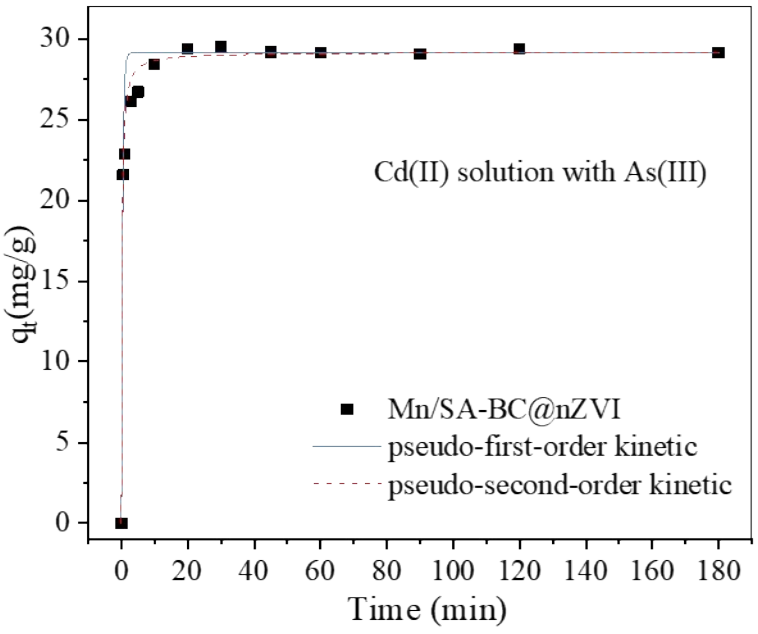

Fig. S11. Cd(II) adsorption kinetics fitted of mixed solution system by pseudo-first-order and pseudo-second-order models.

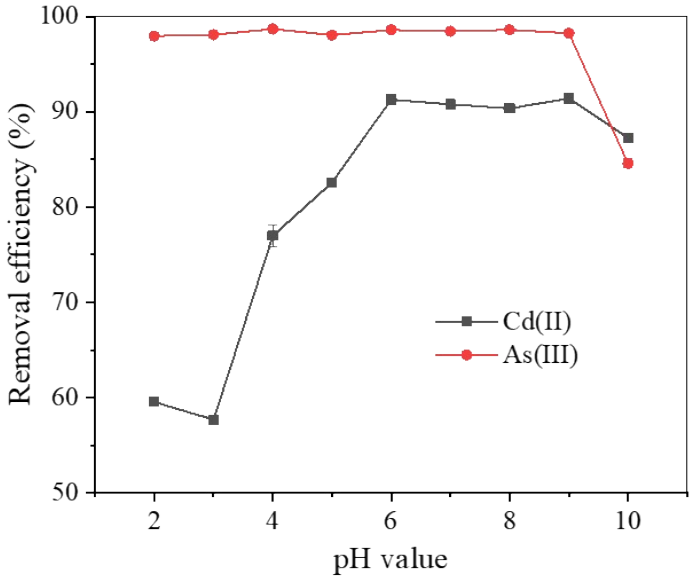

Fig. S12. Effects of initial pH value on the synergistic adsorption of As(III) and Cd(II) by Mn/SA-BC@nZVI.

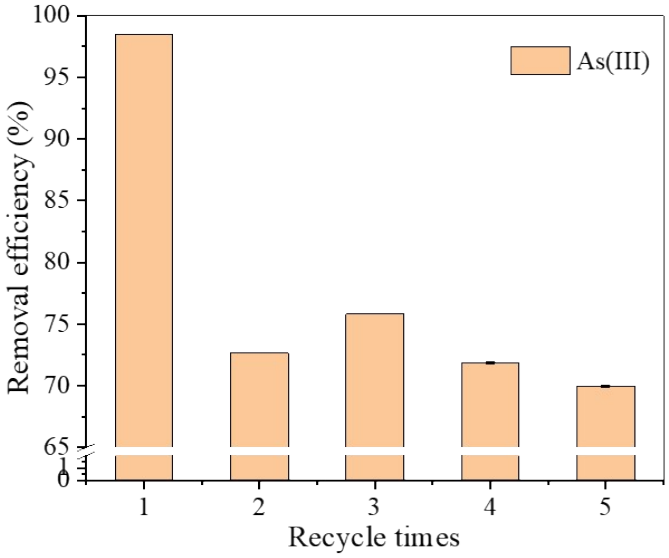

Fig. S13. Removal efficiency of As(III) on Mn/SA-BC@nZVI after repeated adsorption cycles. Initial concentration of As(III): 10 mg/L, respectively, adsorbent dose: 0.5 g/L, shaking speed: 220 rpm, shaking time: 6 h, and temperature: 25°C.

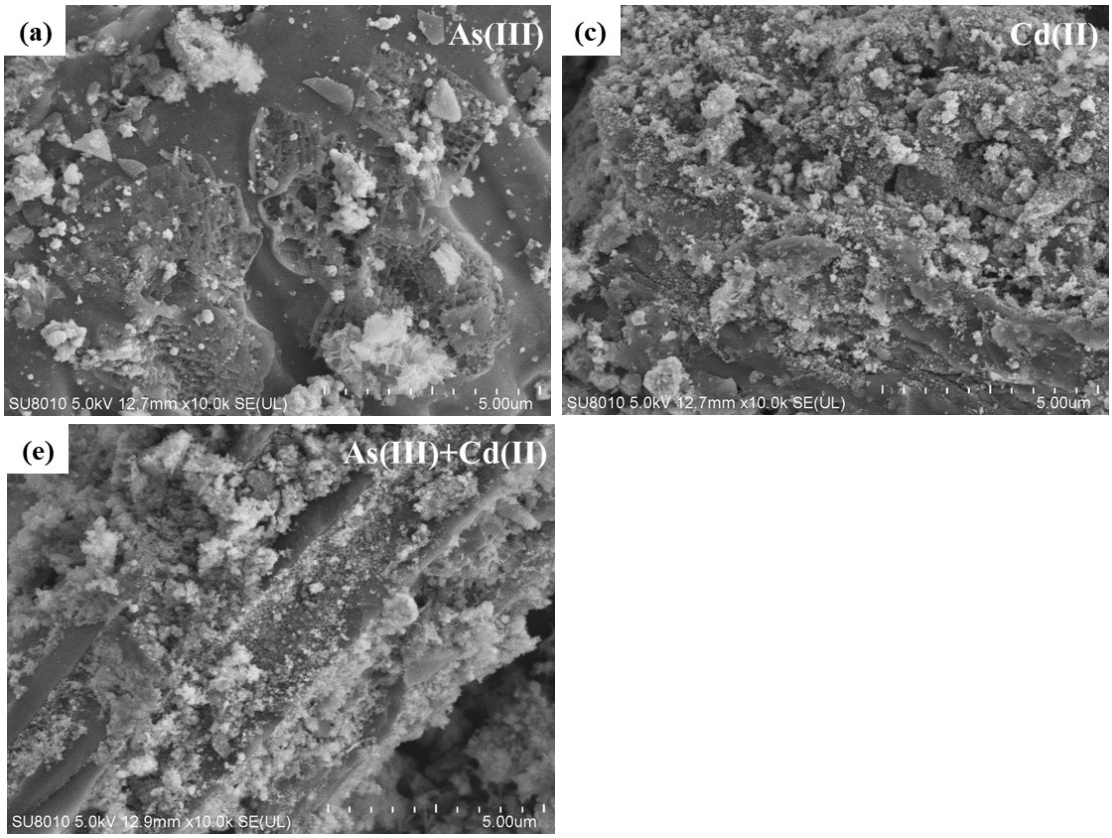

Fig. S14. SEM images results of the samples after Mn/SA-BC@nZVI adsorbed of (a) As(III), (b) Cd(II), and (c) As(III) and Cd(II), respectively.

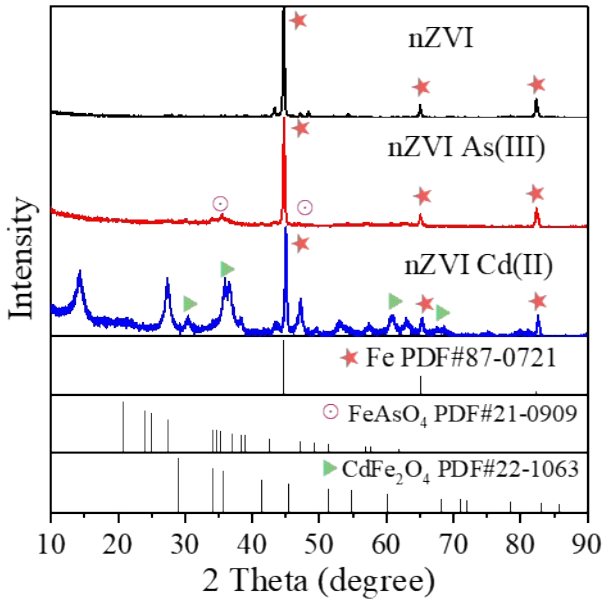

Fig. S15. XRD patterns of nZVI before and after the adsorption of As(III) and Cd(II).

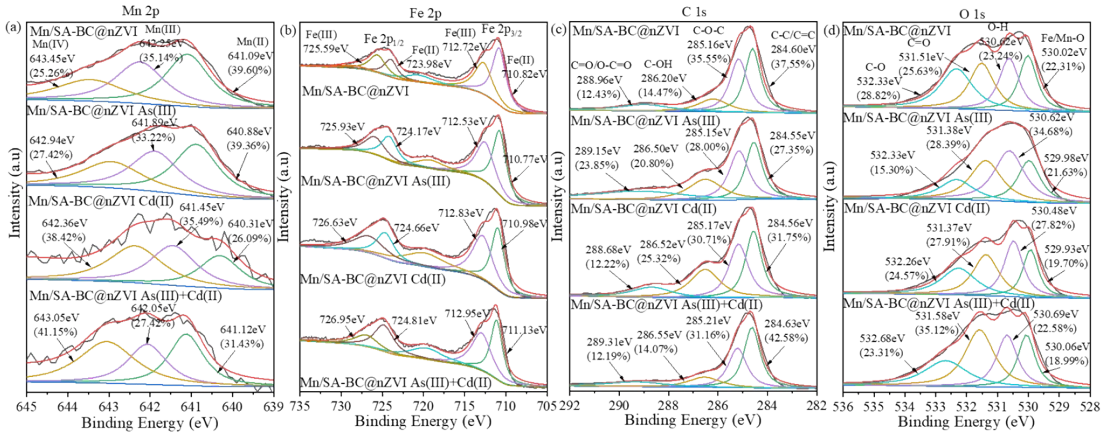

Fig. S16. XPS spectra of (a) Mn 2p, (b) Fe 2p, (c) C 1s, and (d) O 1s of Mn/SA-BC@nZVI before and after adsorption of As(III) and Cd(II).

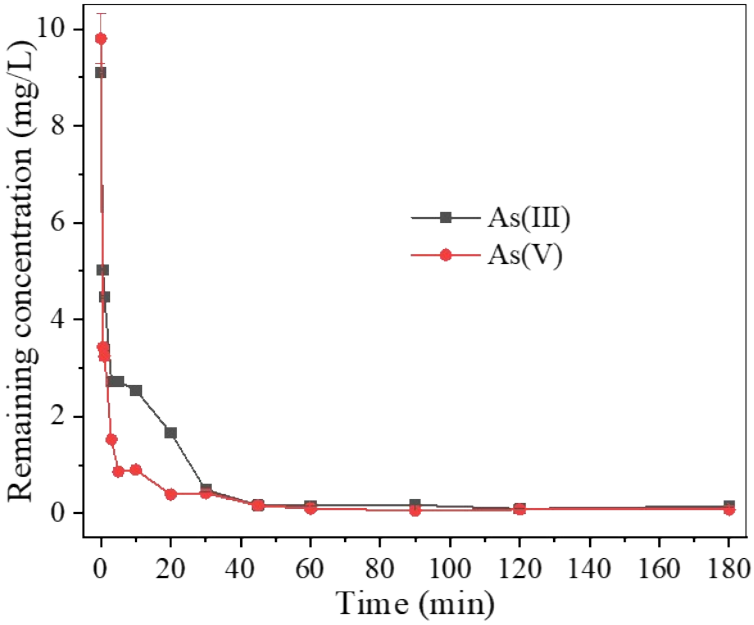

Fig. S17. Adsorption kinetics of As(III) and As(V) on Mn/SA-BC@nZVI. Initial concentration of As(III) or As(V): 10 mg/L, respectively, adsorbent dose: 0.5 g/L, shaking speed: 220 rpm, shaking time: 6 h, and temperature: 25°C.

Notes and references

1. L. Zhang, F. He, W. Mao and Y. Guan, Fast and efficient removal of Cr(VI) to ppb level together with Cr(III) sequestration in water using layered double hydroxide interclated with diethyldithiocarbamate, *Sci. Total. Environ.*, 2020, **727**, 138701.
2. L. Zhang, S. Tang, F. He, Y. Liu, W. Mao and Y. Guan, Highly efficient and selective capture of heavy metals by poly(acrylic acid) grafted chitosan and biochar composite for wastewater treatment, *Chem. Eng. J.*, 2019, **378**.
3. L. Zhang, S. C. Jiang and Y. Guan, Efficient removal of selenate in water by cationic poly(allyltrimethylammonium) grafted chitosan and biochar composite, *Environ. Res.*, 2021, **194**, 110667.
4. G. Yin, X. Song, L. Tao, B. Sarkar, A. K. Sarmah, W. Zhang, Q. Lin, R. Xiao, Q. Liu and H. Wang, Novel Fe-Mn binary oxide-biochar as an adsorbent for removing Cd(II) from aqueous solutions, *Chem. Eng. J.*, 2020, **389**.
5. F. Huang, K. Li, R.-R. Wu, Y.-J. Yan and R.-B. Xiao, Insight into the Cd2+ biosorption by viable Bacillus cereus RC-1 immobilized on different biochars: Roles of bacterial cell and biochar matrix, *J. Clean. Prod.*, 2020, **272**.
6. C. L. Goh, S. Sethupathi, M. J. Bashir and W. Ahmed, Adsorptive behaviour of palm oil mill sludge biochar pyrolyzed at low temperature for copper and cadmium removal, *J. Environ. Manage.*, 2019, **237**, 281-288.
7. T. Yang, Y. Xu, Q. Huang, Y. Sun, X. Liang, L. Wang, X. Qin and L. Zhao, Adsorption characteristics and the removal mechanism of two novel Fe-Zn composite modified biochar for Cd(II) in water, *Bioresource. Technol.*, 2021, **333**.
8. J. Chen, J. Wang, G. Zhang, Q. Wu and D. Wang, Facile fabrication of nanostructured cerium-manganese binary oxide for enhanced arsenite removal from water, *Chem. Eng. J.*, 2018, **334**, 1518-1526.
9. J. Kim, J. Song, S.-M. Lee and J. Jung, Application of iron-modified biochar for arsenite removal and toxicity reduction, *J. Ind. Eng. Chem.*, 2019, **80**, 17-22.
10. Y. Wei, S. Wei, C. Liu, T. Chen, Y. Tang, J. Ma, K. Yin and S. Luo, Efficient removal of arsenic from groundwater using iron oxide nanoneedle array-decorated biochar fibers with high Fe utilization and fast adsorption kinetics, *Water Res*, 2019, **167**, 115107.
11. S. Bakshi, C. Banik, S. J. Rathke and D. A. Laird, Arsenic sorption on zero-valent iron-biochar complexes, *Water Res*, 2018, **137**, 153-163.
12. Y. Feng, P. Liu, Y. Wang, Y. Z. Finfrock, X. Xie, C. Su, N. Liu, Y. Yang and Y. Xu, Distribution and speciation of iron in Fe-modified biochars and its application in removal of As(V), As(III), Cr(VI), and Hg(II): An X-ray absorption study, *J. Hazard. Mater.*, 2020, **384**, 121342.
13. X. Song, Y. Zhang, X. Luo, P. Chen and J. Liu, 2D magnetic scallion sheathing-based biochar composites design and application for effective removal of arsenite in aqueous solutions, *Chem. Eng. Res. Des.*, 2019, **152**, 384-392.
14. L. Wang, Z. Li, Y. Wang, P. C. Brookes, F. Wang, Q. Zhang, J. Xu and X. Liu, Performance and mechanisms for remediation of Cd(II) and As(III) co-contamination by magnetic biochar-microbe biochemical composite: Competition and synergy effects, *Sci. Total. Environ.*, 2021, **750**, 141672.

15. M. Luo, H. Lin, Y. He, B. Li, Y. Dong and L. Wang, Efficient simultaneous removal of cadmium and arsenic in aqueous solution by titanium-modified ultrasonic biochar, *Bioresour. Techno.l*, 2019, **284**, 333-339.
16. D. Yang, L. Wang, Z. Li, X. Tang, M. He, S. Yang, X. Liu and J. Xu, Simultaneous adsorption of Cd(II) and As(III) by a novel biochar-supported nanoscale zero-valent iron in aqueous systems, *Sci. Total. Environ.*, 2020, **708**, 134823.
17. S. Zhu, J. Zhao, N. Zhao, X. Yang, C. Chen and J. Shang, Goethite modified biochar as a multifunctional amendment for cationic Cd(II), anionic As(III), roxarsone, and phosphorus in soil and water, *J. Clean. Prod.*, 2020, **247**.
18. J. Wu, D. Huang, X. Liu, J. Meng, C. Tang and J. Xu, Remediation of As(III) and Cd(II) co-contamination and its mechanism in aqueous systems by a novel calcium-based magnetic biochar, *J. Hazard. Mater.*, 2018, **348**, 10-19.